PAPER

RE$_{16}$Au$_x$Al$_{13-x}$ with RE = La−Nd, Sm ($x \leq 3.37$): synthesis, crystal structure and physical properties of an intermetallic solid solution with barrelane analogue units†

Frank Stegemann[a] and Oliver Janka[*a,b]

During phase analytical investigations in the rare-earth element rich side of the ternary system cerium–gold–aluminum, the new ternary rare-earth (RE) gold aluminides with a composition of RE$_{16}$Au$_x$Al$_{13-x}$ (RE = La−Nd, Sm, $x \leq 3.37$) have been synthesized first by reactive eutectics of RE/Au with Al. Single crystals of high quality can be obtained by this method. The title compounds can be selectively prepared by annealing arc-melted beads of appropriate composition below the peritectic point of the respective system. Like prototypic La$_{16}$Al$_{13}$, the representatives of the solid solution RE$_{16}$Au$_x$Al$_{13-x}$ (RE = La−Nd, Sm; $x \leq 3.37$) crystallize in the hexagonal crystal system (space group $P\bar{6}2m$, a = 916.6–890.4 pm, c = 1122.4–1090.1 pm) with one formula unit per unit cell. Single crystal investigations revealed Au/Al mixing on three of the four crystallographic aluminum sites. These sites form an empty (Au/Al)$_{11}$ barrelane analogous unit, coordinated solely by the respective rare-earth atoms. In addition one independent Al site with a fivefold capped trigonal prismatic arrangement, a so called Edshammar polyhedron, exists. Magnetic measurements of Ce$_{16}$Au$_3$Al$_{10}$ revealed two antiferromagnetic transitions with Neél-temperatures of 7.7(1) and 2.7(1) K and a magnetic moment of μ_{eff} = 2.48(1) μ_B, Pr$_{16}$Au$_3$Al$_{10}$ shows ferromagentic ordering with a Curie-temperature of 19.8(1) K and a magnetic moment of μ_{eff} = 3.58(1) μ_B.

Introduction

The binary phase diagrams of La–Al[1] and Ce–Al[2] contain several intermetallic aluminides. At room temperature the phases RE$_3$Al$_{11}$ (orthorhombic, *Pnma*, La$_3$Al$_{11}$ type),[3] REAl$_3$ (hexagonal, *P*6$_3$/*mmc*, Ni$_3$Sn type),[4,5] REAl$_2$ (cubic, *Fd*$\bar{3}$*m*, MgCu$_2$ type),[6] REAl (orthorhombic, *Cmcm*, CeAl type),[7,8] and RE$_3$Al (hexagonal, *P*6$_3$/*mmc*, Mg$_3$Cd type)[5] exist. In contrast to the other aluminides, RE$_3$Al contains no direct Al–Al contacts due to the low Al content. Additionally, the high temperature phase (La$_{0.88}$Al$_{0.12}$)Al$_2$ with AlB$_2$ type structure exists in the La–Al system between 1363 and 1513 K.[4] This phase has not been found in the Ce–Al system yet. Ce$_3$Al transforms into its β-phase (cubic, *Pm*$\bar{3}$*m*, Cu$_3$Au type) at temperatures above 523 K.[9,10] For this compound also a monoclinic low temperature form (monoclinic, *P*2$_1$/*m*, Ce$_3$Al type) has been found below 115 K.[11] Also HT-LaAl$_4$ and HT-CeAl$_4$, crystallizing in the

BaAl$_4$ type structure (tetragonal, *I*4/*mmm*) have been prepared.[5,6] Finally, La$_3$Al$_2$[12] as well as La$_5$Al$_4$[13] were reported to crystallize in the hexagonal crystal system ($P\bar{6}2m$) with lattice parameters of $a \sim 926$ and $c \sim 1120$ pm. The structure of "La$_5$Al$_4$" was refined from powder X-ray diffraction data and was found to exhibit two mixed occupied crystallographic positions. Niewa and co-workers later reported the crystal structure of La$_{16}$Al$_{13}$ ($P\bar{6}2m$, a = 917 pm, c = 1122 pm),[14] along with physical property measurements and bonding analysis, concluding that their reported composition corresponds to what has previously been reported as La$_3$Al$_2$ and La$_5$Al$_4$. The structure could be refined based on single crystal diffraction data, without any mixed occupational sites. A similar binary cerium compound however has not been reported yet.
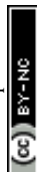
In the ternary system Ce–Au–Al a number of compounds have been found, the majority being Al-rich. Fig. 1 shows the at room temperature stable compounds along with the respective binary compounds. Besides the equiatomic CeAuAl[15] also four members of the solid solution CeAu$_x$Al$_{4-x}$ with x = 1, 1.5, 2 and 2.5 have been reported.[16] Finally CeAu$_3$Al$_7$, obtained from an Al flux reaction, has been reported in 2003 by Latturner *et al.*[17] During exploratory investigations in the rare-earth element rich side of the Ce–Au–Al system, single crystals of Ce$_{16}$Au$_{3.37(1)}$Al$_{9.63(1)}$ (La$_{16}$Al$_{13}$ type, $P\bar{6}2m$, a = 896.47(3),

[a]*Institut für Anorganische und Analytische Chemie, Westfälische Wilhelms-Universität, Corrensstrasse 30, 48149 Münster, Germany.*
E-mail: ocjanka@uni-muenster.de
[b]*Institut für Chemie, Carl von Ossietzky Universität Oldenburg, Carl-von-Ossietzky-Strasse 9-11, 26129 Oldenburg, Germany*
†Electronic supplementary information (ESI) available. See DOI: 10.1039/c6dt02649d
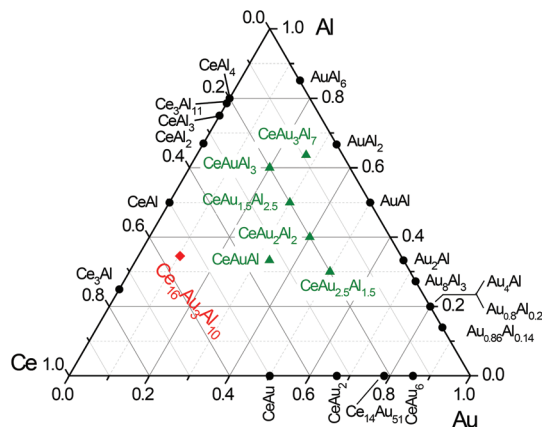
Fig. 1 Isothermic section of the ternary system Ce–Au–Al at room temperature. The known ternary compounds within this system are colored green, the new compound $Ce_{16}Au_3Al_{10}$ is shown in red.

Fig. 2 Thermoanalytical investigation of the nominal composition "Ce_4AuAl" (top) and a stoichiometric sample with the composition $Ce_{16}Au_3Al_{10}$ (bottom).

c = 1097.52(3) pm) could be obtained from an annealed arc-melted button along with the isostructural $La_{16}Au_{2.85(1)}Al_{10.15(1)}$ ($La_{16}Al_{13}$ type, $P\bar{6}2m$, a = 909.09(3), c = 1113.15(4) pm) compound. Herein we report on the synthesis, crystal structures, and thermoanalytical investigations of the title compounds as well as on the physical properties of $RE_{16}Au_3Al_{10}$ with RE = La–Pr.

Results and discussion

Phase diagram and thermoanalytical investigations

In the binary systems Ce–Au, Ce–Al and Au–Al a large number of compounds are known. However only a few ternary representatives have been reported. Especially the rare-earth element rich side of the ternary system Ce–Au–Al has been empty so far. In Fig. 1 the known compounds of the system Ce–Au–Al are shown along with the here reported compound. During investigations of the rare-earth element rich side in this system, single crystals with sizes above 250 μm could be obtained from an annealed arc-melted ingot with a nominal composition of 4-1-1, when searching for new Gd_4RhIn type aluminides.[18] Investigations of the binary phase diagram revealed that at compositions of 84 at% Ce and 16 at% Au and 89 at% Ce and 11 at% Al eutectics with melting points of 793 K and 853 K can be found.[19] Annealing above this temperature therefore enables a reactive flux assisted growth of thermodynamically stable phases. The advantages of metal fluxes for preparative solid state chemistry are well known and have been extensively used to obtain high purity crystals for property investigations.[20]

The obtained crystals have been investigated by single crystal X-ray diffraction (*vide infra*). In order to learn more about this system, thermoanalytical investigations have been performed on pieces of the unannealed 4-1-1 buttons. Two endothermic energy peaks at T_1 = 829 K, T_2 = 845 K are clearly visible upon heating (Fig. 2, top) and two, slightly shifted,
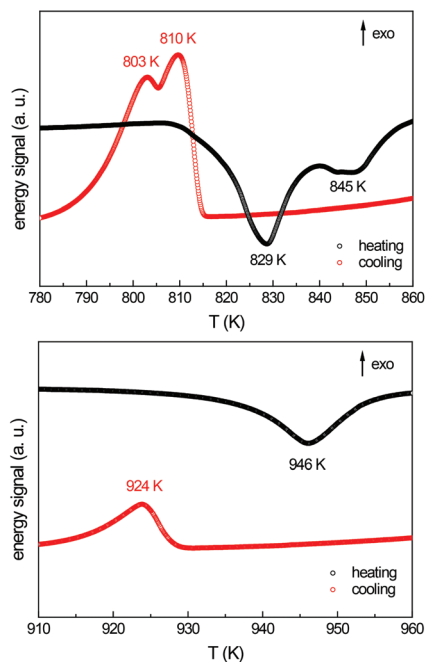
exothermic peaks upon cooling. The endothermic peaks can be interpreted as melting points, the two peaks upon cooling were consequently attributed to be the crystallization of $Ce_{16}Au_{\sim3}Al_{\sim10}$ and the solidification of the remaining melt. In a consecutive step, a fragment of an unannealed button of stoichiometric $Ce_{16}Au_3Al_{10}$ has been investigated with the help of SDT measurements (Fig. 2, bottom). Only one energy peak at T = 946 K can be observed, corresponding to the melting/decomposition of the respective single phase compound. Niewa and co-workers reported $La_{16}Al_{13}$ to melt peritectically at T = 818 K, therefore the specimen prepared for physical property measurements ($RE_{16}Au_3Al_{10}$, RE = La–Pr) were consequently annealed at 823 K, well below the respective melting/decomposition temperature.

Crystal structure

The single crystal data of $La_{16}Au_{2.85(1)}Al_{10.15(1)}$ and $Ce_{16}Au_{3.37(1)}Al_{9.63(1)}$ was refined based on the prototypic crystal structure of $La_{16}Al_{13}$ in the hexagonal crystal system with space group $P\bar{6}2m$ (no. 189).[14] All eight crystallographic sites were identified by Superflip[21] and a correct assignment of the rare-earth and aluminum atoms was achieved in comparison with the literature. The structure was subsequently refined using Jana2006.[22,23] All crystallographic sites occupied by a rare-earth atom are solely occupied by the respective element. However, three of the four crystallographic Al sites, were found to exhibit significantly increased electron density. Those sites were refined as mixed-occupied with gold. These three sites form an 11-atomic [3.3.3]-barrelane analogue unit, while the fourth crystallographic Al site shows no mixed-occupation at
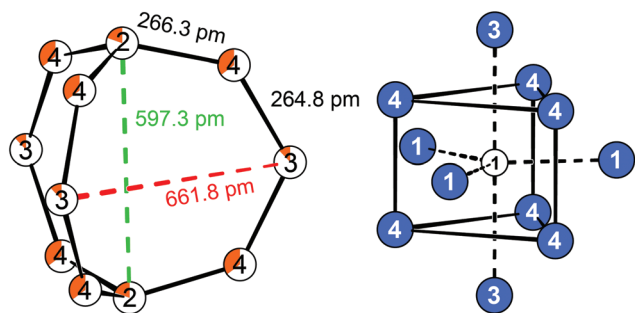
Fig. 3 Coordination environments in the crystal structure of $Ce_{16}Au_3Al_{10}$: (left) eleven atomic [3.3.3]-barrelane-like unit. The segmented spheres represent the mixed occupation by Au (orange) and Al (white). Interatomic distances and distances within the cage are given. (right) Fivefold capped trigonal prism of cerium atoms (blue) surrounding Al1, also known as Edshammar polyhedron (^{11}E).

all. The interatomic distances within the cage-like fragment range between 263–264 pm, which is slightly above the sum of the covalent radii (Al–Al: 250 pm, Au–Al: 259 pm)[24] and close to the shortest distances for binary intermetallic aluminides (Ce_3Al_{11}: Al–Al = 262–291 pm) (Fig. 3, left).

They are also in good agreement compared to $La_{16}Al_{13}$,[14] Tetrakis[bis(trimethylsilyl)methyl]dialan(4), a molecular species with an Al–Al single bond (d(Al–Al) = 266 pm)[25] or to the seven atomic cluster species $[Al_7\{N-(SiMe_3)_2\}_6]^-$ with distances of d(Al–Al) = 277 pm.[26] Within the barrelane unit, the Au/Al2 atom is coordinated by three Au/Al4 atoms. Au/Al3 and Au/Al4 are only twofold coordinated. The Au/Al sites are furthermore coordinated by rare-earth atoms with a total coordination number of 10–12 (Table 4). The isolated Al1 atoms are surrounded symmetrically by eleven rare-earth atoms in the shape of a fivefold capped trigonal prism, also called Edshammar polyhedron, denoted as ^{11}E (Fig. 3, right).[27,28] The Edshammar polyhedra form layers within the ab plane with 1/3 of the polyhedra being absent (Fig. 4).
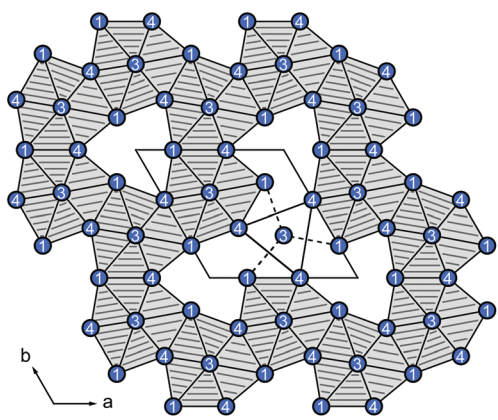

Fig. 4 Layer of Edshammar polyhedra within the ab plane with 1/3 of the polyhedra being absent. The rare-earth atoms are depicted in blue, the Al1 atoms center the polyhedra.
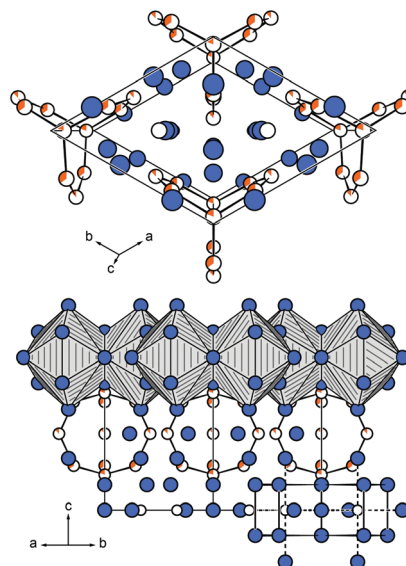

Fig. 5 (top) Central projection of the unit cell of $Ce_{16}Au_3Al_{10}$. (bottom) Stacking of the Edshammar polyhedra layers and the barrelane-like units along the crystallographic c axis. The cerium atoms are shown in blue and the aluminum atoms in open white circles. The segmented parts shown in orange indicate the mixing of aluminum and gold on the respective crystallographic positions.

The [3.3.3]-barrelane units are located above and below the respective voids. They get sandwiched between the layers of Edshammar-polyhedra ($z = 0$ and $z = 1$) whereas the centres of the barrelane units are located at (0, 0, 1/2) (Fig. 5). These cage-like structural fragments, however, are empty with no significant residual electron density. Details of the refinements of the investigated crystals are listed in Tables 2–4. In the case of the cerium compound, a second crystal from a different batch has been investigated by single crystal X-ray diffraction, showing the same composition as well as the same Au to Al distribution on the Au/Al2, Au/Al3 and Au/Al4 sites suggesting the maximum gold content to be close to $x \sim 3$.

Since the investigated compounds have to be viewed as solid solutions, as a consequence more members with different values of x were synthesized. The maximum gold content is evident with respect to the reactive flux syntheses. For both, La and Ce, the single crystals exhibit values of $x \sim 3$, this seems to be the maximum gold content. When using a starting composition RE : Au : Al of 4 : 1 : 1, the remaining melt, after crystallization of the target compound, has to be rich in RE and Au. EDX investigations confirmed this assumption. For $La_{16}Au_xAl_{13-x}$ and $Ce_{16}Au_xAl_{13-x}$ the compounds with x = 1, 2 and 3 were prepared, along with $Pr_{16}Au_3Al_{10}$, $Nd_{16}Au_3Al_{10}$ and $Sm_{16}Au_3Al_{10}$. Interestingly, binary $Ce_{16}Al_{13}$ could not be synthesized; however, $La_{16}Al_{13}$ could be reproduced. The X-ray powder diffraction patterns of the neodymium and samarium samples exhibit reflections being in line with the proposed crystal structure, however significant amounts of by-products were observed. The unit cell of these compounds could be indexed but no phase pure samples for property measure-
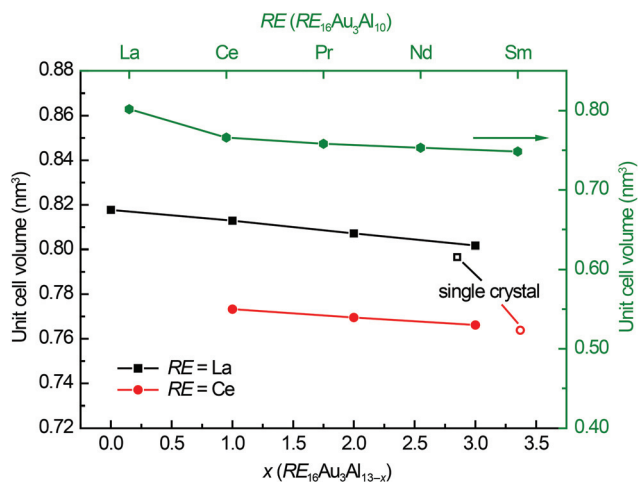
Fig. 6 Unit cell volumes for the members of the solid solutions $La_{16}Au_xAl_{13-x}$ and $Ce_{16}Au_xAl_{13-x}$ plotted *versus* x. Additionally the volumes of $Pr_{16}Au_3Al_{10}$, $Nd_{16}Au_3Al_{10}$ and $Sm_{16}Au_3Al_{10}$ and the course of the volumes of the $RE_{16}Au_3Al_{10}$ (RE = La−Nd, Sm) are shown.

ments could be obtained. The unit cell volumes of all prepared compounds are plotted in Fig. 6; both lattice parameters and unit cell volumes are listed in Table 1. As expected, an almost linear trend is visible in both, the lattice parameters and the unit cell volume. This can be explained by the increasing covalent character of the Au–Al bonds within the barrelane units. When going from lanthanum to cerium, the values shrink again due to the lanthanide contraction. For Pr, Nd and Sm only one compound with x = 3 has been prepared, however the unit cell sizes still fit the expected trend.

Physical properties

$La_{16}Au_3Al_{10}$. The lanthanum representative exhibits Pauli-paramagnetism over the whole temperature range with small susceptibilities of $7.4(1) \times 10^{-3}$ emu mol^{-1} at 300 K, as expected for a compound with no localized moment carrying elements.

$Ce_{16}Au_3Al_{10}$. The top panel of Fig. 7 displays the temperature dependence of the magnetic and inverse magnetic suscepti-
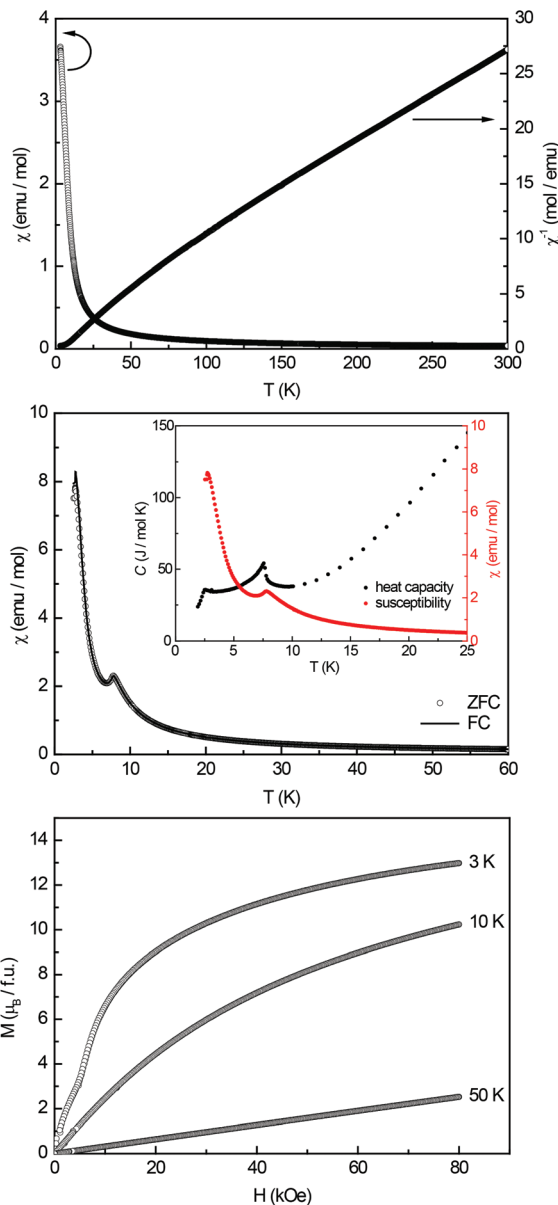
Table 1 Lattice parameters (in pm) and unit cell volumina (in nm^3) for the members of the solid solutions $RE_{16}Au_xAl_{13-x}$ with RE = La−Nd, Sm

	x	a (pm)	c (pm)	V (nm^3)	Ref.
$La_{16}Au_xAl_{13-x}$	0	916.6	1122.4	0.8167	14
	0	917.0(2)	1122.9(2)	0.8177	a
	1	915.1(2)	1120.9(2)	0.8129	a
	2	913.1(2)	1117.9(2)	0.8072	a
	3	911.1(1)	1115.3(1)	0.8018	a
$Ce_{16}Au_xAl_{13-x}$	1	900.2(1)	1102.0(5)	0.7733	a
	2	898.7(2)	1100.3(2)	0.7695	a
	3	897.2(2)	1099.0(3)	0.7662	a
$Pr_{16}Au_xAl_{13-x}$	3	894.1(2)	1094.9(2)	0.7581	a
$Nd_{16}Au_xAl_{13-x}$	3	892.3(3)	1092.4(4)	0.7532	a
$Sm_{16}Au_xAl_{13-x}$	3	890.4(5)	1090.1(6)	0.7485	a

[a] This work.

Fig. 7 Magnetic properties of $Ce_{16}Au_3Al_{10}$: (top) temperature dependence of the magnetic susceptibility χ and its reciprocal χ^{-1} measured with a magnetic field strength of 10 kOe; (middle) magnetic susceptibility in zero-field- (ZFC) and field-cooled (FC) mode at 100 Oe; (inset) comparison of heat capacity measurement and magnetic susceptibility; (bottom) magnetization isotherms recorded at 3, 10 and 50 K.

bility (χ and χ^{-1} data) of $Ce_{16}Au_3Al_{10}$ measured at 10 kOe. A fit of the χ^{-1} data above 100 K using the Curie–Weiss law, revealed an effective magnetic moment of $\mu_{eff} = 2.48(1)$ μ_B per Ce atom and a Weiss constant of $\Theta_p = -33.5(1)$ K. The negative value of the Weiss constant can be attributed to weak antiferromagnetic interactions in the paramagnetic range and to crystal field splitting of the J = 5/2 ground state, which are typically observed for cerium compounds.[29–31] The effective magnetic moment fits well to the theoretical value of 2.54 μ_B for a free

Ce^{3+} ion. To obtain more information about this system, low-field measurements with external field strength of 100 Oe were performed in a zero-field- and field-cooled (ZFC/FC) mode, which are shown in the middle panel of Fig. 7. In comparison to the 10 kOe measurement, showing no magnetic ordering, two antiferromagnetic anomalies can be observed at 2.7(1) K and 7.7(1) K. In order to investigate the origin of the two phenomena, a heat capacity measurement of $Ce_{16}Au_3Al_{10}$, depicted in Fig. 7 (middle, inset), was conducted. In this measurement two anomalies at 2.5(1) and 7.6(1) K are visible as well, suggesting that both magnetic transitions originate from the sample and correspond to two intrinsic antiferromagnetic transitions. This is possible due to four independent cerium sites. The inset of the middle panel of Fig. 7 also shows a comparison of the heat capacity measurement with the magnetic susceptibility underlining that the transition temperatures match well in both measurements. The bottom panel in Fig. 7 displays the magnetization isotherms of $Ce_{16}Au_3Al_{10}$ measured at 3, 10 and 50 K. The isotherm slightly above both ordering temperatures (10 K) displays a curved field dependency of the magnetization as expected for a paramagnetic material. At 3 K the magnetization increases slowly with a spin-reorientation, also called meta-magnetic step, at flux densities <10 kOe. The sharp increase above 10 kOe can be attributed to a ferromagnetic reorientation of the spins, which confirms the antiferromagnetic ground state of the compound. The weak antiferromagnetic (AFM) ground state easily explains the missing transition in the susceptibility measurement at 10 kOe. Here the AFM ground state was destabilized by the applied field. At higher fields almost no tendency for saturation is observed, and the magnetic moment at 3 K and 80 kOe ($\mu_{sat} = 0.81(5)$ μ_B per Ce atom) is much lower than the expected saturation magnetization of 2.14 μ_B according to $g_J \times J$. Such reduced magnetization values often occur in cerium compounds and can be attributed to crystal field splitting of the $J = 5/2$ magnetic ground state of Ce^{3+}.

Electrical resistivity measurements at room temperature indicate metallic character. Upon cooling the resistivity shows irregularities, suggesting micro-cracks in the sample, making a characterization over the full temperature range impossible.

$Pr_{16}Au_3Al_{10}$. The magnetic data of the praseodymium compound is shown in Fig. 8. The top panel displays both magnetic and inverse magnetic susceptibility (χ and χ^{-1} data). From a fit of the χ^{-1} data above 75 K using the Curie–Weiss law, an effective magnetic moment of $\mu_{eff} = 3.58(1)$ μ_B per Pr atom and a Weiss constant of $\Theta_p = 7.5(1)$ K could be calculated. The magnetic moment matches exactly the theoretical moment, the positive value of the Weiss constant can be attributed to weak ferromagnetic interactions in the paramagnetic temperature range. Low-field measurements with external field strength of 100 Oe were performed in a zero-field- and field-cooled (ZFC/FC) mode and are shown in the middle panel of Fig. 8. While the ZFC curve shows characteristics of an antiferromagnetic behaviour the FC curve clearly shows the sign of ferromagnetic coupling. The derivative of the field-cooled data is shown in red with the maximum at $T_C = 19.8(1)$ K.
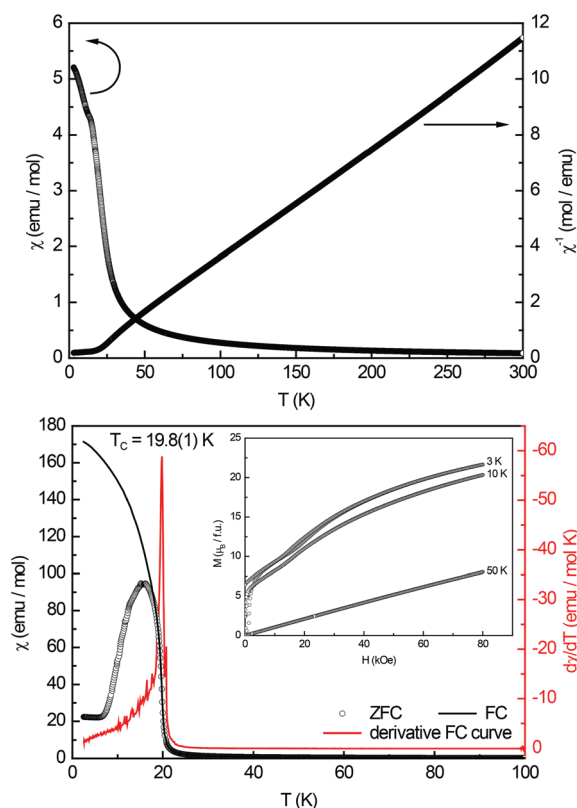
Fig. 8 Magnetic properties of $Pr_{16}Au_3Al_{10}$: (top) temperature dependence of the magnetic susceptibility χ and its reciprocal χ^{-1} measured with a magnetic field strength of 10 kOe; (middle) magnetic susceptibility in zero-field- (ZFC) and field-cooled (FC) mode at 100 Oe along with the dχ/dT curve; (inset) magnetization isotherms recorded at 3, 10 and 50 K.

The magnetization isotherm recorded at 50 K shows a linear field dependency of the magnetization as expected for a paramagnetic material. The 3 K and 10 K isotherms show a strong increase of the magnetization at almost zero field, underlining the ferromagnetic ground state. Near 20 kOe a

Fig. 9 Image of $Ce_{16}Au_{\sim3}Al_{\sim10}$ crystals grown from a sample with a nominal composition Ce_4AuAl. Picture taken by scanning electron microscopy. The residual flux is visible on the left and right hand side.

Table 2 Crystallographic data and structure refinement for $La_{16}Au_{2.85(1)}Al_{10.15(1)}$ and $Ce_{16}Au_{3.37(1)}Al_{9.63(1)}$, space group $P\bar{6}2m$, $Z = 1$

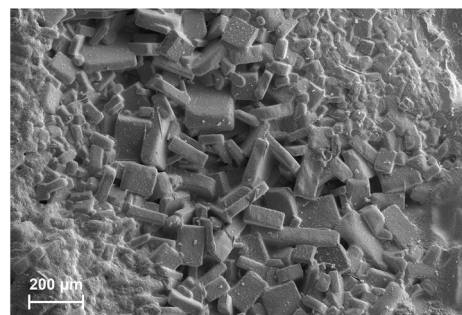| Formula	$La_{16}Au_{2.85(1)}Al_{10.15(1)}$	$Ce_{16}Au_{3.37(1)}Al_{9.63(1)}$
Depository number	431510	431509
Molar mass, g mol^{-1}	3057.7	3165.5
Lattice parameters, pm	$a = 909.09(3)$	$a = 896.47(3)$
	$c = 1113.15(4)$	$c = 1097.52(3)$
Cell volume, nm^3	$V = 0.7967$	$V = 0.7639$
Density calc., g cm^{-3}	6.37	6.88
Crystal size, µm^3	$10 \times 20 \times 20$	$40 \times 60 \times 80$
Diffractometer	StadiVari	IPDS-II
Transm. ratio (max/min)	0.949/0.770	0.338/0.093
Detector distance, mm	40	80
Exposure time, s	4	300
Integr. param. A, B, EMS	5.9, −4.5, 0.012	9.7, 0.5, 0.012
Range in hkl	±14; ±14; ±18	±13; ±13; −14, 16
$F(000)$, e	1269	1319
θ range, °	1.8–35.5	1.9–32.1
Absorption coeff., mm^{-1}	34.2	40.5
No. of reflections	32 688	20 873
Independent reflections, R_{int}	1377/0.1062	1009/0.0759
Reflections with $I > 3\sigma(I)$	978	906
Data/parameters	1377/37	1009/38
Goodness-of-fit	0.87	1.05
R/wR for $I > 3\sigma(I)$	0.0257/0.0490	0.0168/0.0338
R/wR for all data	0.0414/0.0516	0.0227/0.0354
Extinction coefficient	48(12)	159(8)
Flack parameter	0.01(2)	0.01(1)
Largest diff. peak/hole, e Å^{-3}	0.98, −0.91	1.50, −1.36

Further details of the crystal structures investigations may be obtained from the Fachinformationszentrum Karlsruhe, 76344 Eggenstein-Leopoldshafen, Germany (Fax: +49-7247-808-666; E-mail: crysdata@fiz-karlsruhe.de, http://www.fiz-karlsruhe.de/en/leistungen/kristallographie/kristallstrukturdepot/order-form-request-for-deposited-data.html) on quoting the depository numbers given above.

small S-shaped feature appears, typical for a spin-reorientation. This feature remained unclear and might be attributed to trace impurities; however due to the two anomalies observed for $Ce_{16}Au_3Al_{10}$, this magnetic transition might also be intrinsic. At higher fields no tendency for saturation is visible. The magnetic moment at 3 K and 80 kOe reaches $\mu_{sat} = 1.35(5)$ μ_B per Pr atom, which is lower than the expected saturation magnetization of 3.20 μ_B according to $g_J \times J$.

Conclusions

Nine new compounds, $La_{16}Au_xAl_{13-x}$ and $Ce_{16}Au_xAl_{13-x}$ ($x = 1$–3), $Pr_{16}Au_3Al_{10}$, $Nd_{16}Au_3Al_{10}$ and $Sm_{16}Au_3Al_{10}$ crystallizing in the hexagonal $La_{16}Al_{13}$ type structure have been synthesized and structurally characterized. For $La_{16}Au_3Al_{10}$, $Ce_{16}Au_3Al_{10}$ and $Pr_{16}Au_3Al_{10}$ the magnetic properties have been investigated. Single crystals for structural analysis have been grown by the reactive flux method. Ideal synthetic conditions have been obtained with the help of thermoanalytic investigations. The striking feature of the crystal structures are 11-atomic [3.3.3]-barrelane analogue units which get sandwiched between layers build by Al@RE$_{11}$ Edshammar polyhedra. The aluminium positions of the barrelane unit can be substituted with gold up to a maximum of $x \sim 3$. $La_{16}Au_3Al_{10}$ shows Pauli-paramagnetic behaviour, while $Ce_{16}Au_3Al_{10}$ and $Pr_{16}Au_3Al_{10}$ exhibit antiferromagnetic magnetic ordering below $T_N = 7.8(1)$ K and ferromagnetic ordering below $T_C = 19.8(1)$ K respectively.

Table 3 Atom positions and anisotropic displacement parameters (pm^2) for $La_{16}Au_{2.85(1)}Al_{10.15(1)}$ and $Ce_{16}Au_{3.38(1)}Al_{9.67(1)}$. U_{eq} is defined as one third of the trace of the orthogonalized U_{ij} tensor. Coefficients U_{ij} of the anisotropic displacement factor tensor of the atoms are defined by: $-2\pi^2[(ha^*)^2U_{11} + \dots + 2hka^*b^*U_{12}]$. $U_{23} = 0$

Atom	Wyckoff position	x	y	z	U_{11}	U_{22}	U_{33}	U_{12}	U_{13}	U_{eq}
$La_{16}Au_{2.85(1)}Al_{10.15(1)}$										
La1	$3f$	0.25327(10)	0	0	189(3)	159(4)	191(4)	80(2)	0	183(3)
La2	$3g$	0.23043(9)	x	1/2	166(3)	$= U_{11}$	161(3)	101(4)	0	157(3)
La3	$4h$	1/3	2/3	0.66154(7)	158(2)	$= U_{11}$	173(3)	79(1)	0	163(2)
La4	$6i$	0.39061(7)	x	0.16572(6)	176(2)	$= U_{11}$	180(2)	79(2)	−3(2)	181(2)
Al1	$2c$	1/3	2/3	0	131(14)	$= U_{11}$	190(20)	65(7)	0	150(12)
Au/Al2^a	$2e$	0	0	0.2317(2)	155(8)	$= U_{11}$	235(13)	78(4)	0	182(7)
Au/Al3^a	$3g$	0.4203(3)	0	1/2	159(10)	163(14)	178(12)	82(7)	0	166(9)
Au/Al4^a	$6i$	0.28419(10)	0	0.28973(8)	167(3)	188(5)	159(4)	94(2)	0(3)	169(3)
$Ce_{16}Au_{3.37(1)}Al_{9.67(1)}$										
Ce1	$3f$	0.74663(7)	0	0	156(2)	141(3)	137(2)	71(1)	0	146(2)
Ce2	$3g$	0.77163(6)	x	1/2	146(2)	$= U_{11}$	125(2)	93(2)	0	131(2)
Ce3	$4h$	2/3	1/3	0.33775(5)	136(1)	$= U_{11}$	146(2)	68(2)	0	140(1)
Ce4	$6i$	0.61165(5)	x	0.83382(4)	155(1)	$= U_{11}$	155(2)	63(1)	−4(1)	161(1)
Al1	$2c$	2/3	1/3	0	99(9)	$= U_{11}$	106(14)	50(4)	0	102(8)
Au/Al2^b	$2e$	0	0	0.77058(13)	127(5)	$= U_{11}$	197(8)	63(3)	0	150(4)
Au/Al3^b	$3g$	0.5773(2)	0	1/2	125(7)	131(8)	135(8)	66(4)	0	130(6)
Au/Al4^b	$6i$	0.71445(6)	0	0.71128(5)	135(2)	150(3)	119(2)	75(1)	−2(2)	133(2)

^{a} Refined mixed occupations: Au/Al2 − 0.805(4) : 0.195(4); Au/Al3 − 0.881(3) : 0.119(3); Au/Al4 − 0.649(2) : 0.351(2). ^{b} Refined mixed occupations: Au/Al2 − 0.737(4) : 0.263(4); Au/Al3 − 0.864(3) : 0.136(3); Au/Al4 − 0.594(2) : 0.406(2).
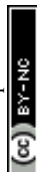
Experimental

Synthesis

Single crystals of $Ce_{16}Au_{3.37(1)}Al_{9.63(1)}$ were first obtained from annealed ingots prepared by arc-melting[32] with a nominal composition "Ce$_4$AuAl" when searching for new Gd$_4$RhIn type aluminides.[18] For the synthesis rare-earth ingots (Sigma-Aldrich, 99.9%), gold shots (Agosi AG, 99.9%), and aluminum turnings (Koch Chemicals, 99.99%) were used. The elements were arc-melted in the $4:1:1$ ratio in a water cooled copper hearth under an argon atmosphere with a pressure of 800 mbar. The argon was purified by molecular sieve and titanium sponge (873 K) to remove traces of water, nitrogen or oxygen. Afterwards, the samples were annealed for 7 d at 1023 K. Due to two intrinsic eutectics with the compositions $Ce_{0.89}Al_{0.11}$ (m.p. 853 K) and $Ce_{0.84}Au_{0.16}$ (m.p. 793 K)[19] crystals of the title compounds could be obtained from the excess melt (Fig. 9). The samples are not stable against diluted hydrochloric or acetic acid; therefore mechanical fragmentation was used to obtain crystals suitable for the structural analysis. This

Table 4 Interatomic distances (pm) for $La_{16}Au_{2.85(1)}Al_{10.15(1)}$ and $Ce_{16}Au_{3.38(1)}Al_{9.67(1)}$. All distances of the first coordination spheres are listed. Standard deviations are equal or smaller than 0.2 pm

$La_{16}Au_{2.85(1)}Al_{10.15(1)}$

La1:	2	Au/Al4	323.7	La2:	1	Au/Al3	317.5	La3:	3	Au/Al3	326.3
	2	Al1	345.2		2	Au/Al3	331.4		3	Au/Al4	332.1
	2	Au/Al2	345.7		4	Au/Al4	333.6		3	La4	340.2
	4	La4	362.5		2	La2	362.8		1	La3	359.6
	2	La4	372.6		2	Au/Al2	364.8		1	Al1	376.8
	2	La1	398.8		2	La4	399.6		3	La2	401.6
					4	La3	401.6				
La4:	1	Au/Al4	326.3	Al1:	6	La4	335.8	Au/Al2:	3	Au/Al4	266.3
	2	Al1	335.8		3	La1	345.2		3	La1	345.7
	2	La3	340.2		2	La3	376.8		3	La4	362.6
	2	Au/Al4	346.6						3	La2	364.8
	2	La1	362.5								
	1	Au/Al2	362.6								
	1	La4	368.9								
	1	La1	372.6								
	1	La2	399.6								
	1	Au/Al3	409.9								
Au/Al3:	2	Au/Al4	264.8	Au/Al4:	1	Au/Al3	264.8				
	1	La2	317.5		1	Au/Al2	266.3				
	4	La3	326.3		1	La1	323.7				
	2	La2	331.4		1	La4	326.3				
	2	La4	409.9		2	La3	332.1				
					2	La2	333.6				
					2	La4	346.6				

$Ce_{16}Au_{3.37(1)}Al_{9.67(1)}$

Ce1:	2	Au/Al4	318.2	Ce2:	1	Au/Al3	312.8	Ce3:	3	Au/Al3	321.7
	2	Au/Al2	339.1		2	Au/Al3	328.5		3	Au/Al4	326.8
	2	Al1	340.4		4	Au/Al4	329.9		3	Ce4	335.3
	4	Ce4	356.4		2	Ce2	354.6		1	Ce3	356.1
	2	Ce4	369.4		2	Au/Al2	360.7		1	Al1	370.7
	2	Ce1	393.4		2	Ce4	393.4		3	Ce2	397.5
					4	Ce3	397.5				
Ce4:	1	Au/Al4	321.8	Al1:	6	Ce4	332.0	Au/Al2:	3	Au/Al4	264.1
	2	Al1	332.0		3	Ce1	340.4		3	Ce1	339.1
	2	Ce3	335.3		2	Ce3	370.7		3	Ce4	355.0
	2	Au/Al4	340.2						3	Ce2	360.7
	1	Au/Al2	355.0								
	2	Ce1	356.4								
	1	Ce4	364.8								
	1	Ce1	369.4								
	1	Ce2	393.4								
	1	Au/Al3	403.6								
Au/Al3:	2	Au/Al4	262.5	Au/Al4:	1	Au/Al3	262.5				
	1	Ce2	312.8		1	Au/Al2	264.1				
	4	Ce3	321.7		1	Ce1	318.2				
	2	Ce2	328.5		1	Ce4	321.8				
	2	Ce4	403.6		2	Ce3	326.8				
					2	Ce2	329.9				
					2	Ce4	340.1				

process was also used to crystallize the isostructural lanthanum compound. The samples are stable against air and moisture for months.

The samples of the solid solutions $RE_{16}Au_xAl_{13-x}$ with RE = La–Nd, Sm and $x = 3$ for magnetic measurements were synthesized by arc-melting the pure elements.[32] The starting materials were weighed in a molar ratio of $16:3:10$ (RE : Au : Al) and arc-melted under argon at 800 mbar. The obtained button was remelted several times to increase the homogeneity. In the final step, the samples were sealed in quartz ampoules and held for 10 d at 823 K, well below the melting point of the compound. The furnace was cooled down to room temperature within 48 h.

Simultaneous differential thermoanalysis (SDT)

Simultaneous Differential Thermoanalytic SDT measurements were carried out on a TA Instruments SDT Q600 instrument. Typically 10 mg of the sample was placed in an Al_2O_3 crucible which was covered with a lid. The samples were transferred into the instrument and heated under a constant Argon stream to 1023 K with a heating rate of 10 K min^{-1} followed by a cooling step to room temperature with the same rate.

X-ray powder diffraction

The polycrystalline samples were characterized by Guinier patterns (imaging plate detector, Fujifilm BAS-1800 scanner) with Cu-Kα1 radiation using α-quartz ($a = 491.30$, $c = 540.46$ pm) as an internal standard. Due to the ductility based on their structural features (*vide supra*) the samples could not be ground to a powder. Consequently the samples were crushed as fine as possible. Correct indexing of the diffraction lines was ensured through intensity calculations using the LAZY-PULVERIX software package.[33] The lattice parameters were obtained through least-squares fits (Table 1).

Single crystal diffraction

Small single crystals were extracted from the crushed annealed ingots or from the flux reactions. The crystals were glued to thin quartz fibers using beeswax and investigated by Laue photographs on a Buerger camera (white molybdenum radiation, image plate technique, Fujifilm, BAS-1800) in order to check their quality. Intensity data sets of four single crystals were collected at room temperature by use of a Stoe IPDS-II image plate system (graphite monochromatized Mo radiation; $\lambda = 71.073$ pm) in oscillation mode or on a four-circle diffractometer (Stoe, StadiVari, μ-source, Mo K$_\alpha$ radiation; $\lambda = 71.073$ pm; oscillation mode) with an open Eulerian cradle setup equipped with a reverse-biased silicon diode array detector (Dectris Pilatus 100 K, resolution: 487 × 195 pixel, pixel size: 0.172×0.172 mm^2).[34] Numerical absorption corrections along with scaling[35] were applied to the data sets. Details of the data collections and the structure refinements of two crystals are listed in Tables 2 and 3.

EDX data

Semiquantitative EDX analyses on all bulk samples and the single crystals used for structure determination were carried out on a Zeiss EVO MA10 scanning electron microscope using La_2O_3, Ce_2O_3, Au and Al_2O_3 as internal standards. The polycrystalline pieces from the annealed arc-melted buttons were embedded in a methylmethacrylate matrix and polished with diamond and SiO_2 emulsions of different particle sizes. The single crystals were measured directly on the quartz fiber. The composition for $La_{16}Au_{2.85(1)}Al_{10.15(1)}$ was determined to 52(2) at% La, 11(2) at% Au, and 37(2) at% Al (theoretical: 55.2 at% La, 9.8 at% Au, and 35.0 at% Al), for the cerium compound $Ce_{16}Au_{3.37(1)}Al_{9.63(1)}$ values of 45(2) at% Ce, 14(2) at% Au, and 41(2) at% Al (theoretical: 55.2 at% Ce, 11.6 at% Au, and 33.2 at% Al) were found. The experimentally observed compositions for the lanthanum compound differ slightly from the theoretical values while for cerium more pronounced deviations are found. These can be explained due to the not perfect perpendicular alignment of the crystals on the fiber with respect to beam and detector. However, phase pure samples with respect to the limitations of the instrument were observed after annealing. No impurity elements heavier than sodium (detection limit of the instrument) were observed.

Physical properties measurements

Polycrystalline pieces of the annealed $RE_{16}Au_3Al_{10}$ button were packed in kapton foil and attached to the sample holder rod of a Vibrating Sample Magnetometer unit (VSM) for measuring the magnetization $M(T,H)$ in a Quantum Design Physical-Property-Measurement-System (PPMS). The sample was investigated in the temperature range of 2.5–300 K and with magnetic flux densities up to 80 kOe.

For the heat capacity measurement from 1.9–300 K, a piece of the sample used for the susceptibility measurements (4.551 mg) was fixed to a pre-calibrated heat capacity puck using Apiezon N grease.

Acknowledgements

Notes and references

1 H. Okamoto, *J. Phase Equilib. Diffus.*, 2007, **28**, 581–581.
2 H. Okamoto, *J. Phase Equilib.*, 1998, **19**, 395–396.
3 A. H. Gomes de Mesquita and K. H. J. Buschow, *Acta Crystallogr.*, 1967, **22**, 497–501.
4 J. H. N. van Vucht and K. H. J. Buschow, *J. Less-Common Met.*, 1966, **10**, 98–107.
5 K. H. J. Buschow, *Philips Res. Rep.*, 1965, **20**, 337–348.
6 H. N. Nowotny, *Z. Metallkd.*, 1942, **34**, 22–24.

7   C. Bècle and R. Lemaire, *Acta Crystallogr.*, 1967, **23**, 840–845.

8   A. Leineweber and H. Jacobs, *J. Alloys Compd.*, 1998, **278**, L10–L12.

9   A. Iandelli, *Natl. Phys. Lab. (U. K.), Symp.*, 1951, 3F-2-3F11.

10 J. H. N. van Vucht, *Z. Metallkd.*, 1957, **48**, 253–258.

11 A. C. Lawson, J. M. Lawrence, J. D. Thompson and A. Williams, *Physica B*, 1990, **163**, 587–590.

12 N. F. Chaban and Y. B. Kuz'ma, *Dokl. Akad. Nauk SSSR, Ser. A*, 1971, **11**, 1048–1050.

13 N. M. Belyavina, V. Y. Markiv and V. V. Zavodyanny, *J. Alloys Compd.*, 2004, **367**, 132–136.

14 R. Niewa, M. Kirchner, H. Zhang, W. Schnelle and Y. Grin, *Z. Kristallogr.*, 2005, **220**, 115–121.

15 F. Hulliger, *J. Alloys Compd.*, 1993, **200**, 75–78.

16 F. Hulliger, *J. Alloys Compd.*, 1995, **218**, 255–258.

17 S. E. Latturner, D. Bilc, J. R. Ireland, C. R. Kannewurf, S. D. Mahanti and M. G. Kanatzidis, *J. Solid State Chem.*, 2003, **170**, 48–57.

18 F. Tappe, C. Schwickert, S. Linsinger and R. Pöttgen, *Monatsh. Chem.*, 2011, **142**, 1087–1095.

19 T. B. Massalski, H. Okamoto, P. R. Subramanian and L. Kacprzak, *Binary Alloy Phase Diagrams*, ASM International, Ohio, U.S.A., 2nd edn, 1990.

20 M. G. Kanatzidis, R. Pöttgen and W. Jeitschko, *Angew. Chem., Int. Ed.*, 2005, **44**, 6996–7023.

21 L. Palatinus and G. Chapuis, *J. Appl. Crystallogr.*, 2007, **40**, 786–790.

22 V. Petříček, M. Dušek and L. Palatinus, *Jana2006. The crystallographic computing system*, Institute of Physics, Praha, Czech Republic, 2006.

23 V. Petříček, M. Dušek and L. Palatinus, *Z. Kristallogr.*, 2014, **229**, 345–352.

24 J. Emsley, *The Elements*, Clarendon Press, Oxford University Press, Oxford, New York, 1998.

25 W. Uhl, *Z. Naturforsch., B: Chem. Sci.*, 1988, **43**, 1113–1118.

26 A. Purath, R. Köppe and H. Schnöckel, *Angew. Chem., Int. Ed.*, 1999, **38**, 2926–2928.

27 S. Lidin, T. Popp, M. Somer and H. G. von Schnering, *Angew. Chem., Int. Ed. Engl.*, 1992, **31**, 924–927.

28 L.-E. Edshammar, *X-ray studies on binary alloys of aluminium with platinum metals*, Stockholm University, Sweden, 1969.

29 W. Hermes, R. Mishra, U. C. Rodewald and R. Pöttgen, *Z. Naturforsch., B: Chem. Sci.*, 2008, **63**, 537–542.

30 B. Chevalier and J. L. Bobet, *Intermetallics*, 2001, **9**, 835–838.

31 P. Javorský, L. Havela, V. Sechovský, H. Michor and K. Jurek, *J. Alloys Compd.*, 1998, **264**, 38–42.

32 R. Pöttgen, T. Gulden and A. Simon, *GIT Labor-Fachz.*, 1999, **43**, 133–136.

33 K. Yvon, W. Jeitschko and E. Parthé, *J. Appl. Crystallogr.*, 1977, **10**, 73–74.

34 Dectris, *Technical Specification and Operating Procedure Pilatus 100K-S Detector System, Version 1.7*, 2011.

35 Stoe & Cie GmbH, *X-Area (Version 1.70)*, 2014.